Article

International Journal of Micro Air Vehicles

Micro air vehicles energy transportation for a wireless power transfer system

International Journal of Micro Air Vehicles
Volume 11: 1–13

DOI: 10.1177/1756829319870057
journals.sagepub.com/home/mav
SAGE

Jose Polo, Lluís Hontecillas, Ignacio Izquierdo and Oscar Casas

Abstract

The aim of this work is to demonstrate the feasibility use of an Micro air vehicles (MAV) in order to power wirelessly an electric system, for example, a sensor network, using low-cost and open-source elements. To achieve this objective, an inductive system has been modelled and validated to power wirelessly a sensor node using a Crazyflie 2.0 as MAV. The design of the inductive system must be small and light enough to fulfil the requirements of the Crazyflie. An inductive model based on two resonant coils is presented. Several coils are defined to be tested using the most suitable resonant configuration. Measurements are performed to validate the model and to select the most suitable coil. While attempting to minimize the weight at transmitter's side, on the receiver side it is intended to efficiently acquire and manage the power obtained from the transmitter. In order to prove its feasibility, a temperature sensor node is used as demonstrator. The experiment results show successfully energy transportation by MAV, and wireless power transfer for the resonant configuration, being able to completely charge the node battery and to power the temperature sensor.

Keywords

MAV, Unmanned aerial vehicle (UAV), wireless power transfer, sensor network

Received 30 October 2018; accepted 25 July 2019

Introduction

The applications of Micro air vehicles (MAV) are growing every year. One of these applications is measurement and monitoring.[1–5] The MAVs can be used to transport any type of payload, from parcels[6] to sensors,[7] mobile node sensors or to transport the data collected by static sensor nodes.[8] In this last scenario, sensor nodes cannot communicate among them, hence, they need assistance to send the measured data. The MAV can pick up the data and transport to destination. Furthermore, the MAV can transport others payloads, as energy when the sensors are located in low-energy environments or harsh environments, for instance, a battery is inadequate in extremely hot environments,[9] the sensor node can capture the energy carried by the MAV. These nodes are non-battery sensor nodes. In addition, the tendency is that they are low cost and open source.[10]

Thus, the sensor network is composed of two node types: a mobile node that integrates an MAV and several static nodes containing the sensors. There are many examples of applications that use this type of networks: monitoring bridges,[11] Internet of things,[12] agriculture[8] and many more.

In order to simplify the energy transfer from mobile node to static node, a wireless transfer is used. Although the idea of wireless power transfer (WPT) began in 19th century, it is necessary to wait until the early 1970s where experiments with RFID tags were done by the U.S. government,[13] and by the early 2000s the Professor She Yuen developed a charger to provide resonant power transfer for small electronics.

Recently, in 2007, MIT researchers were able to power a 60-W light bulb from a power source while providing 40% efficiency over distance in excess of 2 m using resonant inductive coupling.[14] Until that

Electronic Engineering Department, Universitat Politècnica de Catalunya, Barcelona, Spain

Corresponding author:
Jose Polo, Universitat Politècnica de Catalunya, Esteve Terradas, 7, Castelldefels, Barcelona 08860, Spain.
Email: jose.polo@upc.edu

moment, the maximum transfer distances achieved between transmitter and receiver were on centimeter range scale. This event signified a turning point in WPT systems. In July 2010, wireless charging technology for portable electronic devices up to 5 W reached commercialization stage through launching the Qi Standard by the Wireless Power Consortium,[15] now comprising more than 220 companies worldwide.

The main limitation for this energy transfer technique is the distance. It is only efficient for short distance. Instead of expending great resources to improve the efficiency with large distances, it is much easier to transport energy wherever is needed, shortening distance. MAVs can carry energy anywhere, reducing the distance to values where this energy transfer technique is efficient.[16–20] have several examples of this application to sensor networks.

Different optimizations have been introduced. In case of large node number, the optimization is oriented to determine scheduling priority for charging requests when multiple nodes are waiting for charging.[21–23] Other optimization takes into account not only the distance but also the angle between the energy receiver and the charger's orientation.[24] There are applications in which the path medium is not air. For instance, in the case of implanted devices, the tissue media introduces path losses.[25] WPT systems using a resonant frequency are more efficient that those do not use it. It is possible to use a single frequency or multiple frequencies.[26]

The ideal solution is to use large coils to obtain great efficiency, but it is not possible to use in an MAV. The main goal of this work is the study and development of a small WPT system, adapted to the dimensions and conditions imposed by the UAV, so that it does not suffer major changes in its dynamics. Furthermore, this work demonstrates the use of MAV for energy transportation in order to shorten the distance for an efficient WPT. This development is done using low-cost and open-source components and devices.

In order to demonstrate that accomplish these constraints, an application has been developed. The system architecture consists of several modules: MAV, energy transmitter, energy receiver and sensor node, see Figure 1. The energy transmitter and receiver modules have been developed. The other modules are commercial ones. Those modules are described in the next sections.

The design is easily adaptable to any other MAV system with any other electric system.

WPT systems

WPT works by modulating the generated electric, magnetic or electromagnetic fields to transport power from a transmitter towards a receiver at certain distance.

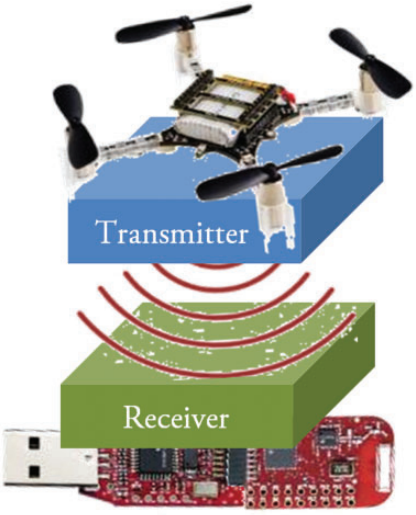

Figure 1. Demonstrator system. It is composed of, from top to bottom, an MAV, an energy transmitter, an energy receiver and a sensor node.

There are two main types: the near-field transfers and the far-field transfers. The first one is divided into capacitive and inductive couplings, and the second one into propagating electromagnetic, microwave and photo-electricity. Table 1 summarizes several characteristics between near-field, nonradiative and far-field, radiative techniques.

Efficiency is a desired characteristic, thus nonradiative techniques, near-field, were selected. Capacitive coupling was rejected because of safety issues related to the necessity of a high-source voltage. Magnetic fields interact so weakly with biological organisms, it is also important for safety considerations.[28]

Model of resonant magnetic induction

A changing magnetic flux through a surface bounded by a closed stationary loop of wire induces an electric current in the wire. This current is also found in a static magnetic field, when a changing magnetic flux is created by a moving loop of wire through the surface bounded by the wire itself.

The magnetic flux, $\varnothing_m$, through a surface is the surface integral of the normal component of the magnetic field, $\vec{B}$, passing through that surface. Our system uses two loops: one to generate the magnetic field (transmitter), the other where the current is induced in it (receiver). In our case, these surfaces are defined as the transmitter and receiver loops, see Figure 2. These loops are formed by several turns, forming coils. As magnetic field is proportional to the number of field lines per area unit, the magnetic flux is proportional to the number of field lines through an area element.[29] Since the coil surface is

Table 1. Comparison among the wireless power transfers.[27]

WPT system	Frequency	Directivity	Range	Efficiency
Capacitive coupling	Low: Hz–MHz	Weak	Short	High
Inductive coupling	**Low: Hz–MHz**	**Weak**	**Short**	**High**
Propagating electromagnetic	Med.: MHz–GHz	Medium	Medium	Medium
Microwave	High: GHz–THz	Strong	Long	Low
Photo-electricity	High: >THz	Strong	Long	Low

Note: Inductive coupling was selected, highlighted in bold.

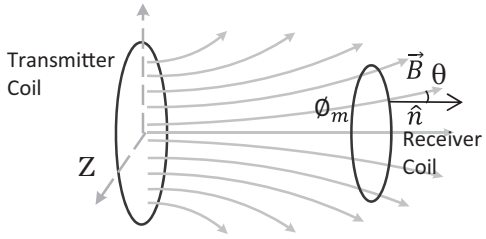

Figure 2. Magnetic field, $\vec{B}$, lines from transmitter or primary coil generate magnetic flux, $\varnothing_m$, on the receiver or secondary coil.

flat, has a constant area, A, and has several turns, N, if we assume magnetic field is uniform in magnitude and direction everywhere on the area, the magnetic flux through the coil area is

$$\varnothing_m = \vec{B} \cdot \hat{n} A = N\ B\ A\ \cos\ \theta \tag{1}$$

where θ is the angle between the direction of $\vec{B}$ and the direction of the unit vector normal to the coil surface, $\hat{n}$, see Figure 2.

Equation (1) shows that flux can be modified altering B, A, N or θ. A, N and θ correspond to the coil geometry. For an existent coil, it is easier to modify B than the geometry. Thus, it is necessary to use alternating current (AC) that generates a magnetic field that changes in time. The result of this variation of magnetic flux is an electro motive force, ε, induced along the path that is equal in magnitude to the rate of change of the magnetic flux through the surface. This is known as Faraday's law

$$\varepsilon = -\frac{d\varnothing_m}{dt} \tag{2}$$

According to the Faraday's law, the polarity of the induced magnetic field is such that it produces a magnetic field that opposes the change which produces it. Because of induced voltage and current are produced at the secondary side, power is successfully transferred from the primary to the secondary side. This is the basic working principle of the inductive coupling.

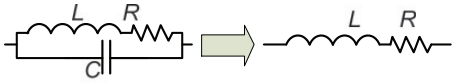

Figure 3. Coil circuit models.

Coreless transformer modelling

In order to study the coils to be used in the inductive coupling, it is necessary to use an electric model of a coil. It is made of copper wire, thus, the coil, in addition to inductive behaviour, has resistive and capacitive behaviours; for this reason, the coil model used is composed by an inductance, a resistance and a capacitance, see Figure 3, left. The coil inductance L itself, the resistance R is the effective resistance of the conductor of the coil at the operating frequency. The capacitance C accounts for the end-to-end and turn-to-turn stray capacitance of the coil.[30] This capacitance is due to the fact that the inductor is made out of a coil of insulated wire. Therefore, tiny capacitors are created between the windings since there are two sections of conductor separated by an insulator.

In our case, the capacitance is small enough and can be neglected, thus the model is composed by an inductance and a resistance, Figure 3, right.

Coil resistance R

At low frequencies ($f < 200\,\text{kHz}$),[31] the resistance experiments a DC behaviour. Its value only depends on the wire geometry and material. The DC resistance of a metal conductor is given by

$$R_{DC} = \rho \frac{l}{S} \tag{3}$$

where l is the wire length (m), S is the wire section (m^2) and ρ is the electrical resistivity of the metal material (Ω·m). For copper, the most usual metal used, is $1.68 \cdot 10^{-8}\,\Omega$·m.

When the frequency increases up to 200 kHz, some effects appear that increase the wire resistance with the frequency. The resistance behaves as an AC resistance due to the *skin-effect* and *proximity-effect*.

Skin-effect happens in all wire and cable. When the signal is DC, the current uses the entire conductor, with the same amount of current flowing in the inner part as on the outer part of the wire. As the frequency is increased, the current density is larger near the surface of the conductor and decreases with greater depths in the conductor. Consequently, the equivalent cross-section decreases and the wire resistance is increased with frequency. To quantify the skin-effect, the *skin-depth*, δ, is introduced. It is a measure of how far electrical conduction takes place in a conductor and is a function of frequency, no matter how thick the wire is

$$\delta = \frac{1}{\sqrt{\pi f \mu \sigma}} \tag{4}$$

where σ is the electrical conductivity $(1/\rho)$ of the wire material (S/m), f is the frequency (Hz) and μ is the total permeability in free space and in material ($\mu = \mu_0 \cdot \mu_m$).

The resistance corresponding to skin-effect can be calculated as

$$R_{skin} = R_{DC}\frac{4d}{\delta} \tag{5}$$

where d is the diameter of the conductor.

Moreover, there is another phenomenon that increases the resistance of a conductor when an AC is applied. It is the *proximity-effect*. This effect is the apparent resistance increment of the wire due to the circulating current in the conductor caused by the alternating flux of other nearby conductors. As a result, more power losses appear in the windings. To quantify the proximity-effect, the Dowell's assumption[32] is used

$$R_{proximity} = R_{DC} \cdot \Psi\left[\frac{\sinh(2\Psi)+\sin(2\Psi)}{\cosh 2\Psi - \cos(2\Psi)} + \frac{2}{3}(N^2-1)\frac{\sinh(2\Psi)-\sin(2\Psi)}{\cosh 2\Psi + \cos(2\Psi)}\right] \tag{6}$$

where N is the number of turns of the coil and Ψ can be obtained by

$$\Psi = \left(\frac{100d}{2\delta}\right)\sqrt{\pi} \tag{7}$$

The total equivalent resistance is

$$R_{EQ} = R_{DC} + R_{skin} + R_{proximity} \tag{8}$$

Coil inductance L

Inductors with solid-core provide better coupling than air-core ones, but a limitation of our system is the weight transported by the MAV. The primary coil is wanted to go on a micro quadcopter, thus, air-core coils are used instead of solid-core ones.

To calculate the coil inductance, Wheeler's formula can be used for air-cored inductor[33]

$$L = KDN^2 \cdot 10^{-9}\ [\mathrm{H}] \tag{9}$$

where K is a parameter that depends on the dimension ratio (D/l) of the coil, where l is the length of the coil, whose value is listed in appendix 11.A of Chen,[33] D is the diameter of the coil and N is the number of turns.

WPT modelling

The WPT comprises of two coils: a primary transmitter coil (T_x) and a secondary receiver coil (R_x). The coils are modelled with a resistance and an inductance as seen above. Figure 4 shows this model that contains three voltage generators: V_s is the generator of the power to transmit; $j\omega Mi_1$ and $j\omega Mi_2$ take into account the mutual inductance (M) of the coils. Furthermore, the model includes the resistances and inductances of the coils (R_1, L_1, R_2 and L_2) and the load resistance (R_L) of the device to be powered.

The influence of the secondary coil in the primary one can be viewed as a reflected impedance (Z_R). Its value comprises the impedance of the secondary coil and the mutual inductance

$$Z_R = \frac{\omega^2 M^2}{R_2 + R_L + j\omega L_2} \tag{10}$$

Figure 5 shows the equivalent circuit with the reflected impedance. The power transferred to the reflected impedance is given by

$$P_{out} = \frac{V_{out}^2}{Z_R} \tag{11}$$

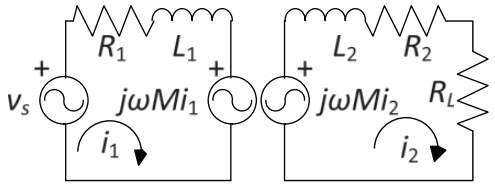

Figure 4. Primary and secondary coil models.

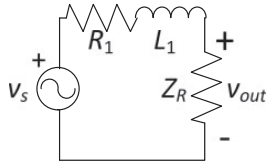

Figure 5. Equivalent circuit with reflected impedance.

V_{out} can be calculated as

$$V_{out} = V_s \frac{Z_R}{Z_1 + Z_R} \tag{12}$$

where

$$Z_1 = R_1 + j\omega L_1 \tag{13}$$

then

$$P_{out} = V_S^2 \frac{Z_R}{(R_1 + j\omega L_1 + Z_R)^2} \tag{14}$$

The maximum power transfer occurs when $Z_R = Z_1$. This result is a restrictive parameter since Z_R depends on the mutual inductance, which in turn depends on the distance between the transmitter and receiver coil. Thus, there is no a unique optimal value of Z_1.

This system has an important energetic drawback: secondary coil impedance is usually high; therefore, when the power transferred to the load is intended to be increased, the input voltage should be also increased, provided that P_{out} is proportional to the square of V_s. But this solution is not optimal because it requires higher current amplitudes in the primary coil, and therefore greater Joule losses.[31] In order to solve this disadvantage, resonance capacitors are added to the primary and secondary circuits. They cancel (or decrease notably) the large reactance of a coil by working at the resonant frequency. These capacitors allow to reduce the current amplitudes and to improve the efficiency of the coreless transformer. The intrinsic capacitances of the coils (see Figure 3) are negligible, but these capacitors are necessary in order to minimize the large reactance of the coils. These capacitors have a much higher capacity than the intrinsic capacities of the coils.

A circuit containing an inductor and a capacitor has a resonant frequency (f_0). When this circuit works at that frequency, the inductive and capacitive reactances are equal in magnitude. Then they cancel and the resistance only contributes to the impedance. This one has a minimum value. Below that natural frequency, the resonance circuit looks capacitive, since the impedance of the capacitor increases while inductive reactance decreases. Above resonance frequency, the circuit behaves oppositely.

There are four resonant configurations, see Figure 6. They are labelled as SS, SP, PS and PP. The first letter indicates for the primary, the second one for the secondary. S or P indicates series or parallel for the capacitor. The generators taking into account the mutual inductance of the coils (see Figure 4) are not represented in order to simplify the figure.

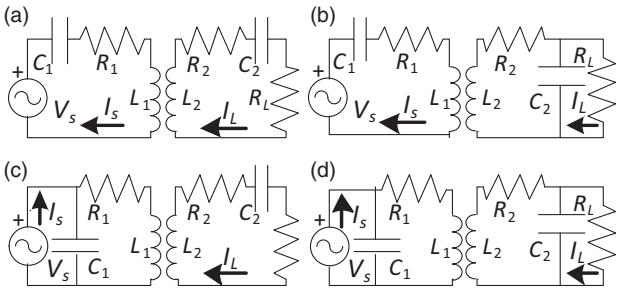

Figure 6. Four resonant configurations. The generators of the mutual inductance *M*, Figure 4, are not represented in order to simplify the figure. (a) SS, (b) SP, (c) PS and (d) PP.

The input power P_{in} and the load power P_L are

$$P_{in} = V_s \cdot I_s \cdot \cos(\varphi) \tag{15}$$

$$P_L = I_L^2 \cdot R_L \tag{16}$$

where φ is the phase between the input voltage, V_S, and the primary current, I_S. P_{in} is multiplied by the power factor, $\cos(\varphi)$, which corresponds to compute the active or consumable power.

In order to select the best topology, the efficiency ($\eta = P_L/P_{in}$) and the output power is studied versus the resonant frequency (f_0).

Figure 7 shows the efficiency (η), left, and the output power (P_L), right, for all topologies. It can be seen that the greater the efficiency, the lower the bandwidth. From the results, it can be concluded that the best topologies are SS and SP. PP topology has a better efficiency than SS and SP at the resonant frequency, but the output power is much lower.

It is not possible to determine the ideal operating frequency without knowing many factors as coil sizes, self-resonant frequency, efficiency, etc. Hence, it is intended to determine the suitable frequency band where the coils could work properly. The upper limit is restricted by the maximum switching frequency of the power driver used to drive the transmitter coil. Other high frequency limitation is the coil self-resonance frequency (f_s) and the parasitic capacitance of the coils (see Figure 3). Exciting the windings with a frequency of about 10% f_s ensure that the parasitic capacitive effects will not influence the inductor impedance values.[34] Due to the fact that the experimental results of f_s are not higher than 30 MHz, the upper limit for maximal operating frequency is set to be 3 MHz.

For low frequencies, there are no restrictions, but recommendations. The Wireless Power Consortium suggests as admissible, quality factor, $Q = \omega L/R$,

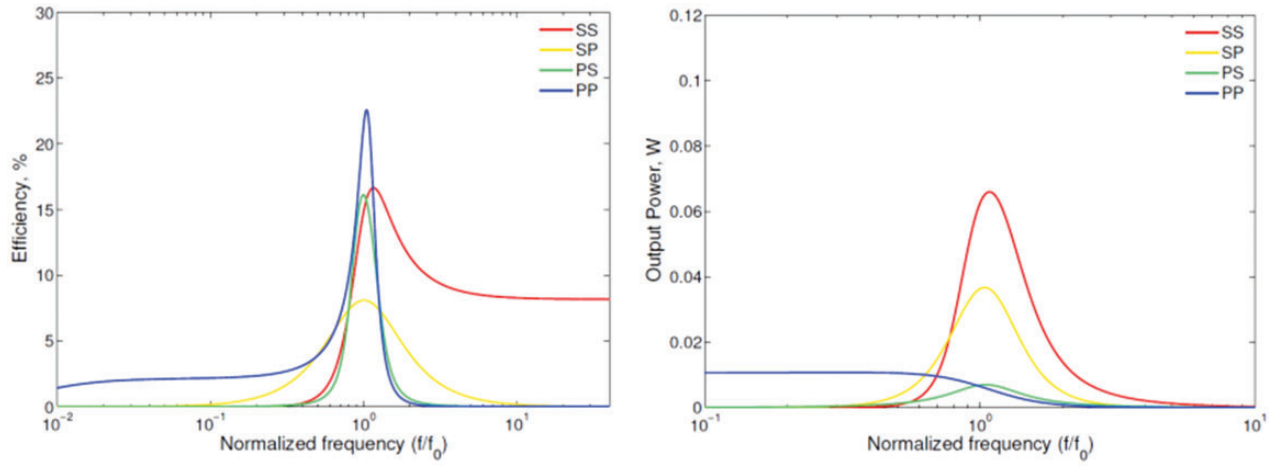

Figure 7. Efficiency, (η), left, and output power, (P_L), right, versus the normalized resonant frequency.

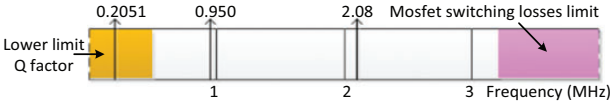

Figure 8 Frequency bands constrains. Frequency references: 0.2051 MHz,[35] 0.950 MHz,[36] 2.08 MHz.[37]

values above 100 for WPT applications. To achieve the desired Q factor, frequencies higher than 500 kHz are typically needed.

Figure 8 shows the specific frequency band for coils' diameters between 3 cm and 10 cm, which is the desired order of magnitude of the coils due to drone size. The vertical arrows indicate frequencies (MHz) used in different works with similar characteristics as ours.[35–37] The selected frequency should be some units of Mega Hertz. In our case, 1 MHz was selected due to drone size limitations, and it is easy and cheap to generate using a quartz crystal, which is stable and permits a narrow band.

Hardware design of WPT

As Figure 1 shows, the system is composed of an MAV, a transmitter unit and a receiver unit.

MAV

One of the initial objectives of the project is the WPT system outfitting on the micro quadcopter, remember that one objective is the use of low-cost elements. The inclusion of the quadcopter as an energy transporter restricts transmitter and receiver sides because of the weight and dimension. The coils must be designed taking into account the constraints imposed by the drone.

The model used in this work is created by Bitcraze, its second micro quadcopter version, named Crazyflie 2.0, see Figure 9. It is one of the smallest quadcopter in the market. It is ideal for indoor and environments with obstacles. It measures 9.2 cm from helix to helix and weighs 27 g. It has a flight autonomy around 7 min at full thrust. Its maximum recommended payload weight is 15 g, and it supports up to 42 g of weight at take-off.

Figure 9. Micro quadcopter Crazyflie, left, and USB dongle, right.

It has two microcontrollers. The main one is used to execute the main application; it is a built-in ARMCortex-M4 processor, STM32F405. This processor has a 32-bit architecture and can work until 168 MHz. The second microcontroller is used to manage the power and the radio. This is an ARM Cortex-M0 microprocessor, nRF51822, that works at 32 MHz. Furthermore, it has an inertial measurement unit, MPU-9250, which is composed of a gyroscope of three axes, an accelerometer of three axes and a magnetometer of three axes. They provide 9 degrees of freedom. Additionally, it has a barometer to measure atmospheric pressure, LPS25H, and a temperature sensor.

The quadcopter has two modules: the quadcopter itself, Figure 9 left, and an USB dongle, right, for its control.

Crazyflie 2.0 is an open-source quadcopter. Its firmware is based on FreeRTOS.[38] It is an operating system for embedded devices. Crazyflie 2.0 can be controlled by three methods: from an Android device using an application, from a PC using a Python application that permits using a joystick and a Python library that permits sending orders to the quadcopter.

Transmitter and the receiver circuits

The main feature of the WPT system lies on energy conversion. Hence, the transmitter and the receiver circuits need power converters. Figure 10 shows the WPT system architecture. The power stored in a battery is conditioned for using by the transmitter coil. The power captured by the receiver coil is conditioned again for using by the load.

Coil characteristics

Typical shapes of WPT inductors include circular, square, rectangular and all regular polygons. Circular coils obtain a higher magnetic coupling than any other shape. This can be explained by the distortion of the field distribution around the corners of those shapes.[39]

Each conductor has a different electrical resistivity which is an important parameter to define its DC and AC resistance. The most common metal used is copper. It is easy to obtain and it has a relatively low resistivity, $1.68 \times 10^{-8}\,\Omega\cdot$m. It is used as a wire of 0.59 mm diameter, with polymeric layer insulation, 1.4 mm total diameter, because of its ease to obtain.

The dimensions are restricted by the payload of the MAV. Its maximum take-off weight is 42 g. The drone will carry other devices than the coil, and therefore, we limit the coil weight to 15 g. The coil radius is restricted by the drone dimension to 5 cm maximum.

Three different coils were constructed to be tested to select the best candidate. Table 2 shows the dimensions of those coils. Model A corresponds to the maximum size allowed by the drone. As we said above, midrange WPT applications contain distances from coil diameter up to 10 times the coil diameter.[40] Thus, if we aspire to transfer power up to 40 cm, at least a coil with 4 cm of diameter is needed. This is the diameter of model B. Model C corresponds to an intermediate size.

Both Tx and Rx coils were designed with the same dimensions for each of models A, B and C. This assumption simplifies computations and coil winding procedures.

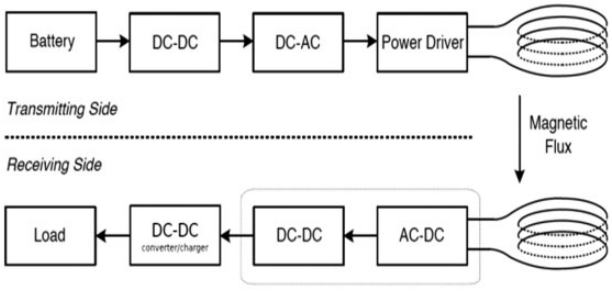

Figure 10. WPT system architecture.

Transmitting side

The transmitting subsystem is carried by the micro quadcopter. It has a battery for its powering. In order to simplify the system and avoiding increasing the total weight, it was decided to use one battery to give power to the transmitting coil and to the drone. The battery voltage is 3.7 V, and to increase power without having to use large current, voltage was increased. Figure 10 shows the different parts of the transmitter power adapter. The DC–DC converter raises from 3.7 V to 12 V. A switching regulator (TPS61088) is used to raise the voltage. It has an efficiency of about 92%.

Table 2. Dimensions of coils.

Model name	Turns	Radius (cm)	Mass (g)
A	8	5	13.4
B	19	2	14.1
C	10	4	13.5

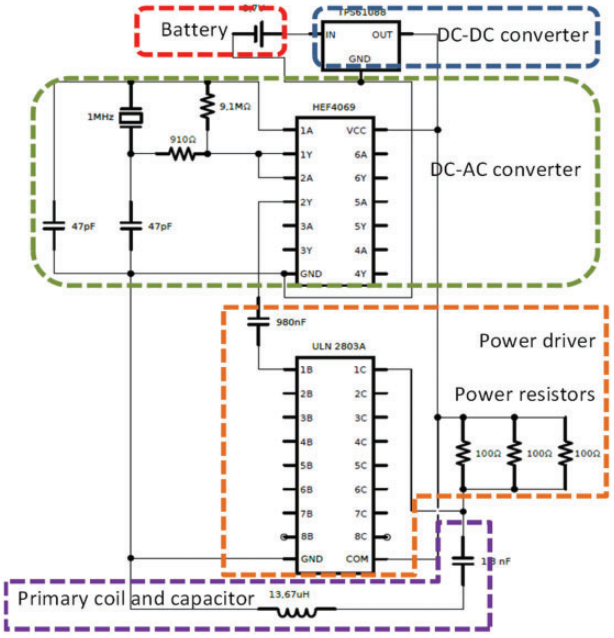

Figure 11. Electric schematic of the transmitter module. It is composed of a battery, a DC–DC converter, a DC–AC converter, a power driver and the primary coil and capacitor.

The DC–AC converter (HEF4069) is an oscillator that prepares the voltage to attack the coil. It converts the 12 V DC to AC.

The power driver is used to increase the current given to the coil. It is composed of Darlington transistors (ULN2803A) and power resistors. In our case, this current was 0.32 A. The maximum given power to the coil was around 3.8 W.

Figure 11 shows the electric schematic of the transmitter module. It is composed of the components detailed above and the primary coil and capacitor.

Figure 12 shows the assembled transmitter circuit containing the previous explained subsystems. It has the appropriate dimension to fit the droid.

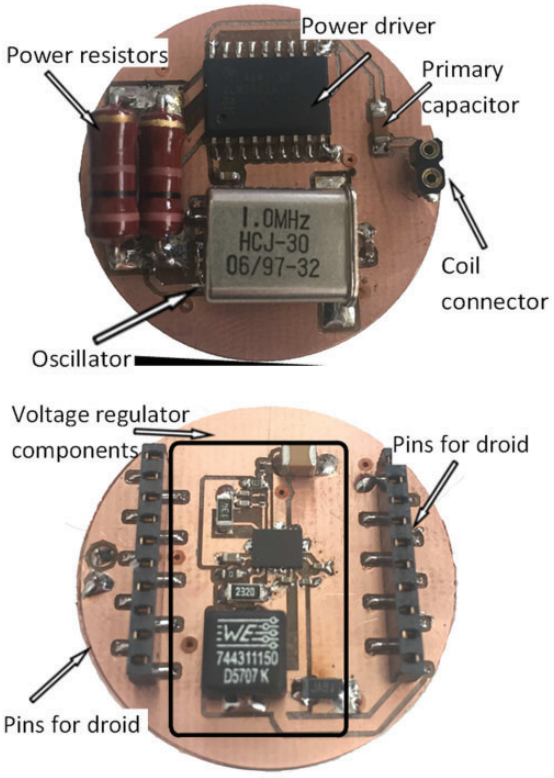

Figure 12. Transmitter circuit, see Figure 10 transmitter side. Top view, above, bottom view, below.

Receiving side

The receiving subsystem has to adapt the captured power by the receiving coil. Figure 10 shows the different parts of the transmitter power adapter. It rectifies the received AC voltage to DC. It is composed of Schottky diodes. They can switch at the working frequency of 1 MHz.

The DC voltage has to set it up to the desirable voltage level. A DC–DC boost converter (bq25504EVM) is used to increase the voltage. Then it is stored in a storage element for its use. The storage element can be a battery or a capacitor. In our case, a capacitor was chosen, of 140 mF.

Figure 13 shows the electric schematic of the receiver module. It is composed of the components detailed above and the secondary coil and capacitor, and the sensor node. Figure 14 shows the assembled receiver circuit containing the previous explained subsystems.

In order to demonstrate the system viability, a simple wireless sensor node was selected: eZ430-RF5000T. This device is a wireless developing tool with an integrated temperature sensor. An eZ430-RF5000T board is connected to the receiver and wirelessly communicates with other board which is

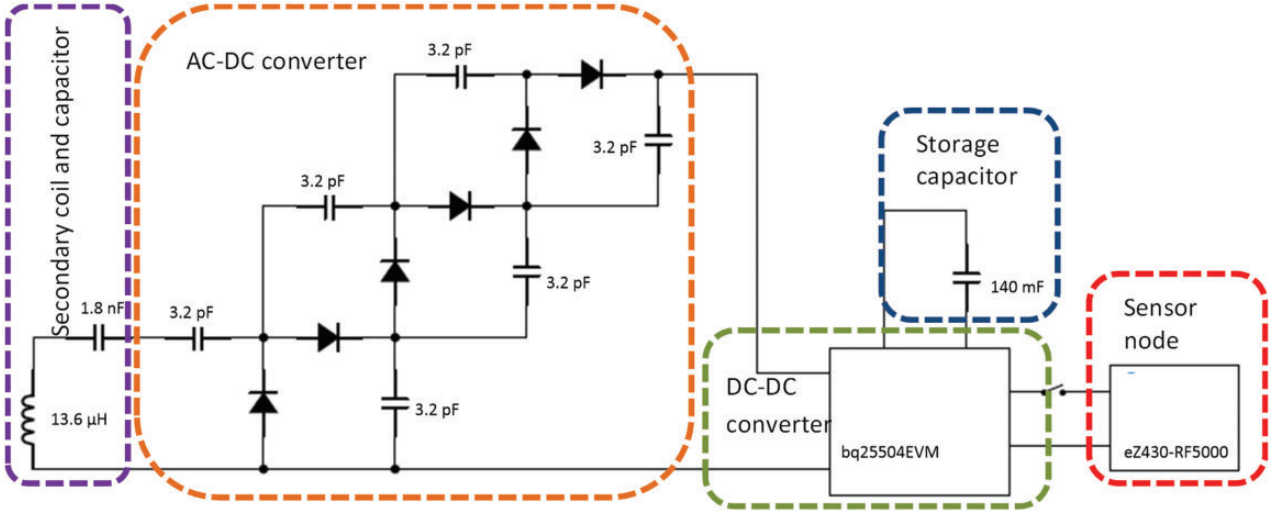

Figure 13. Electric schematic of the receiver module. It is composed of the secondary coil and capacitor, an AC–DC converter, a DC–DC converter, a storage capacitor and the sensor node.

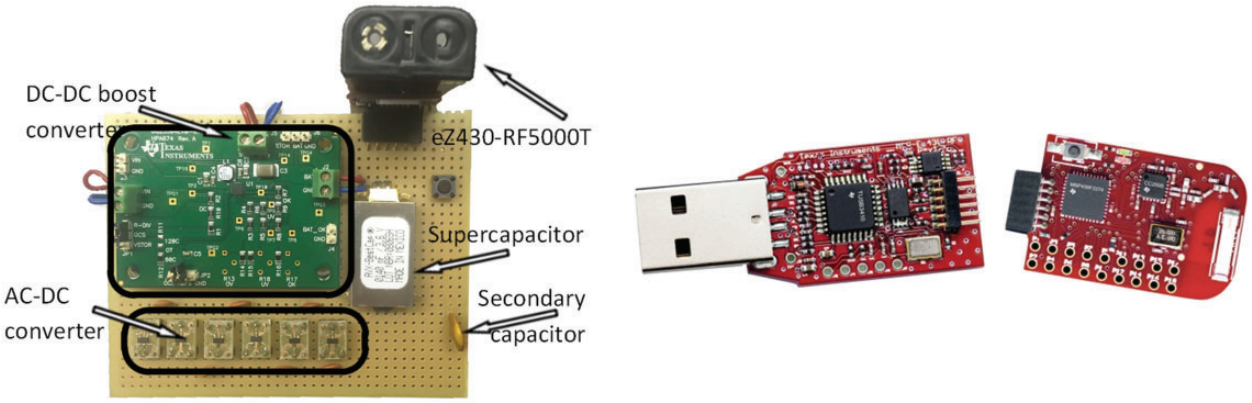

Figure 14. Receiver circuit, see Figure 10 receiver side, left. eZ430-RF5000T board, right.

connected via USB to a computer. The eZ430-RF5000T measures the air temperature and sends it to the board connected to the computer. The temperature is shown on the computer screen.

The eZ430-RF5000T consumption, when in active mode, is about 270 μA. But it needs 21.2 mA to wireless communication. This current can be easily supplied by the selected supercapacitor.

Experimental measurements

Several measurements have been done to test the previous designs.

Coil characteristics

Each coil is characterized by a resistance and an inductance, see Figure 3. They have been measured using an Agilent 4294 A Precision Impedance Analyzer (40 Hz–110 MHz). All voltage measurements are done using an Agilent DSO3062A oscilloscope and several Agilent N2862A probes. Figure 15 shows the measurement setup with two coils of model C, the probes and the oscilloscope.

Table 3 shows the measured and calculated values for the three coil models, A, B and C, see Table 2. Tx is for transmitter coils and Rx for receiver coils. Calculated values are obtained using equations (8) and (9).

In order to select the proper coil model, several measurements have been carried out using the various configurations described above: SS and SP resonant configurations, see Figure 6, using the different model coils, see Table 2. The power is measured on the receiver coil to select the best configuration. Table 4 shows only several of the measures obtained in order to clarify this selection.

The measurement setup is the following:

- Exciting voltage: 1 Vrms, correspond to Vs in Figure 6.

Figure 15. Coil measurement set-up.

- Frequency: 0.7 MHz, 1 MHz and 2 MHz. Only the results for 1 MHz are shown in Table 4.
- Distance between coils: from 2.5 cm to 10 cm. Only the results for 3.8 cm are shown in Table 4.

Table 4 shows that the best coil model is A, but C has similar results, although slightly lower. Regarding the resonant configuration, SP is better than SS. The A model is better than the C model, but the first one is larger, 10 cm in diameter, instead of 8 cm for C. This smaller model is better for coupling to the quadcopter

and it allows better flight control and less rolling. Therefore, C coil and SP configuration are selected.

Figure 16 shows the power received and the efficiency as a function of distance for SP topology and C coils. It compares the theoretical power received calculated using equation (16) and the measured one. The theoretical curve is higher than the experimental one because the model does not take into account some losses. It can be seen that, as expected, the smaller the distance, the greater the power received. Therefore, the drone should be placed as close as possible to improve the transfer of energy.

Table 3. Measurements and calculations of resistance and inductance for each model coil.

	Resistance (Ω)		Inductance (μH)	
Coil model	Measured	Calculated	Measured	Calculated
ATx	0.5639	0.6519	12.45	12.38
ARx	0.5916	0.6519	12.46	12.38
BTx	0.6071	0.6193	13.96	12.72
BRx	0.6380	0.6193	13.70	12.72
CTx	0.6704	0.6519	13.67	13.26
CRx	0.6286	0.6519	13.67	13.26

Note: The calculated values are obtained using equations (8) and (9).

Table 4. Power (mW) received on the secondary using different resonant configuration and different coil model.

Resonant configuration \ Coil model	A	B	C
SS	3.4	1.3	3
SP	6	2.6	5

System performance

A test was carried out to determine the autonomy of the micro quadcopter battery using the transmitter circuit coupled to the receiver, and charging the super capacitor without the load installed. As it was seen previously, the closer are the coils, the more efficient is the energy transfer. The tests were done using different distances between coils, from 2.5 cm to 7 cm. It is difficult to maintain a quadcopter in static flight, and to facilitate its positioning, it has pillars in order to maintain its position and avoid to waste battery energy using the quadcopter engines. In order to perform the tests, several pillars with different lengths were used. In order to facilitate the landing, we can attach a small camera to the UAV and a tag at the centre of the coil. Then it is possible to land manually, looking for the tag, or automatically using the Open CV library.[41] The full charging of the super capacitor in minimum time was obtained at a distance of 2.5 cm, it was at 10 min with the micro quadcopter battery without being discharged completely. Longer times were obtained with larger distances: 4 cm was 26 min, 6 cm 88 min and 7 cm 2.5 h. The micro quadcopter's battery is completely discharged after 15 min approximately, see Figure 17. The horizontal dashed line indicates the voltage limit where the inductive system is turned off. This limit corresponds to the minimum voltage allowed by the regulator to boost the voltage level to 12 V_{DC}.

The same test has been tested with the SS topology and the charge time is increased over 14 min. This test experimentally confirms that the optimal topology to use is the SP compensation topology.

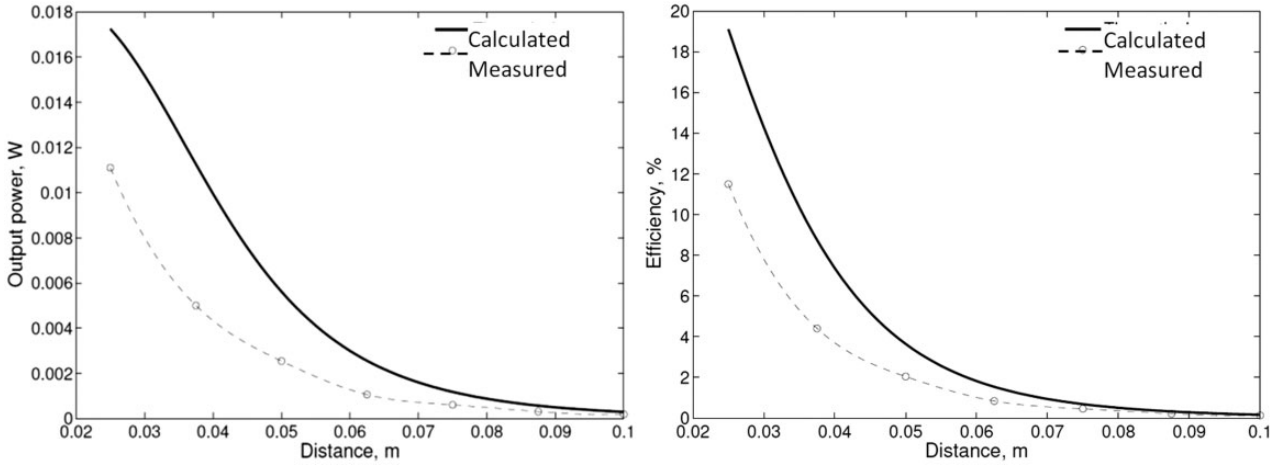

Figure 16. Power received and efficiency vs. distance for SP topology and C coils.

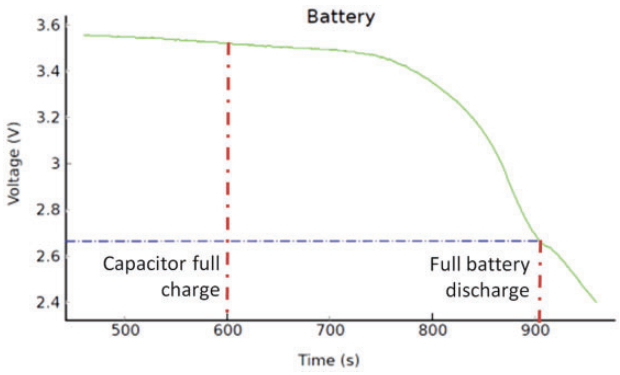

Figure 17. Micro quadcopter's battery discharging evolution.

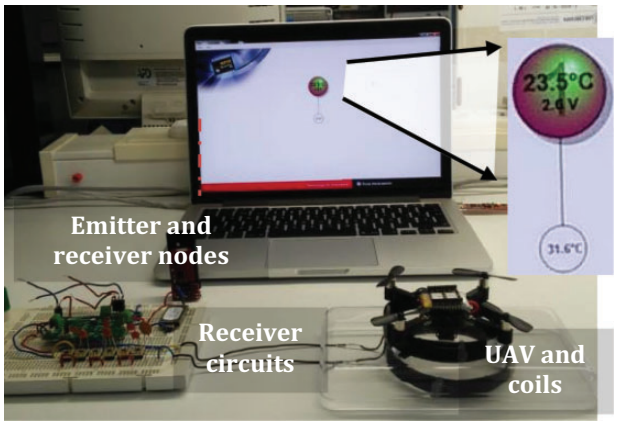

Figure 18. System performance measurement set-up: receiver circuits, left down; emitter and receiver nodes, left; MAV and coils, right down; PC, centre.

Figure 18 shows the experimental set-up for these measurements. The quadcopter and the coils can be seen on the lower right area. The transmitter coil is located on the bottom part of the quadcopter in order to facilitate magnetic coupling with the secondary coil; furthermore, this placement, on the lower part of the quadcopter, facilitates its transportation and improves the quadcopter stability.

The secondary coil is settled apart from the node and receiver circuits; this layout permits a better coupling with the primary coil and allows that the nodes can have the adequate setting to correctly carry out the measurements.

Behind them, there is a computer that has connected a node. This node receives the data transmitter from the emitter node, the one that is powered from the secondary coil. The computer screen shows the temperature received, and on the right there is a detail of the temperature display.

Conclusions

This work demonstrates the feasibility of using a micro quadcopter for wireless energy transfer using magnetic induction to supply energy to a sensor node, using open-source elements, resulting in a low-cost system.

The use of a resonant circuit is necessary to improve the energy transfer efficiency. Three different coils and four different circuits have been studied, simulated and implemented. Measurements have confirmed the results calculated.

Several conditioning circuits have been used to adapt the energy saved in the micro quadcopter battery to be transmitted by the coils, and then saved again in the node supercapacitor in order to supply the sensor node. Coil sizes and working frequency have been optimized for using with the Crazyflie. Energy has been transmitted from the Crazyflie to a sensor node.

Our system is capable to charge the super capacitor in 10 min, at 2.5 cm, using a coil of 4 cm of radius and 13.5 g of weight, allowing the node sensor to send the temperature wirelessly.

This work shows the methodology and characteristics that the coils and circuits must accomplish in order to WPT and the MAV to transport the system. All components are low-cost elements. Using these directives, any other system can be designed, with any other dimensions.

Declaration of conflicting interests

The author(s) declared no potential conflicts of interest with respect to the research, authorship, and/or publication of this article.

Funding

The author(s) received no financial support for the research, authorship, and/or publication of this article.

ORCID iD

Jose Polo https://orcid.org/0000-0002-9917-1795

References

1. Rashed S and Soyturk M. Effects of UAV mobility patterns on data collection in wireless sensor networks. In: *IEEE international conference on communication, networks and satellite (COMNETSAT)*, 10–12 December 2015. Bandung, West Java, Indonesia.
2. Meivel S, Gandhiraj N, Dinakaran K, et al. Remote sensing for urea spraying agricultural (UAV) system. In: *International conference on advanced computing and communication systems (ICACCS -2016)*, Coimbatore, India, 22–23 January, 2016.
3. Lin H, Huang H, Lv Y, et al. Micro-UAV based remote sensing method for monitoring landslides in three gorges reservoir, China. In: *IEEE international geoscience and*

remote sensing symposium (IGARSS), Beijing, China, 10–15 July 2016.
4. Say S, Inata H, Liu J, et al. Priority-based data gathering framework in UAV-assisted wireless sensor networks. *IEEE Sensors J* 2016; 16: 5785–5794.
5. Ma X, Kacimi R and Dhao R. Fairness-aware UAV-assisted data collection in mobile wireless sensor networks. In: *International wireless communications and mobile computing conference (IWCMC),* Cyprus, Paphos, 5–9 September 2016.
6. Hochstenbach M, Notteboom C, Theys B, et al. Design and control of an unmanned aerial vehicle for autonomous parcel delivery with transition from vertical take-off to forward flight. *Int J Micro Air Veh* 2015; 7: 395–405.
7. González Toro F and Tsourdos A. *UAV sensors for environmental monitoring*. Special issue UAV sensors for environmental monitoring. 2018.
8. Polo J, Hornero G, Duijneveld C, et al. Design of a low-cost wireless sensor network with UAV mobile node for agricultural applications. *Comput Electron Agric* 2015; 119: 19–32.
9. Aqueveque P, Morales AS, Saavedra F, et al. Temperature monitoring of electrolytic cells using wireless battery-free harsh environment sensors. In: *IEEE industry applications society annual meeting,* Portland, Oregon, USA, 2–6 October 2016.
10. Manecy A, Marchand N, Ruffier F, et al. X4-MaG: a low-cost open-source micro-quadrotor and its linux-based controller. *Int J Micro Air Veh* 2015; 7: 98–109.
11. Johnson J, Basha E and Detweiler C. Charge selection algorithms for maximizing sensor network life with UAV-based limited wireless recharging. In: *2013 IEEE eighth international conference on intelligent sensors, sensor networks and information processing*, 2–5 Apr 2013. Melbourne, Australia.
12. Sharma V, Kumar R and Kaur R. UAV-assisted content-based sensor search in IoTs. *Electron Lett* 2017; 53: 5–25.
13. Roberti M. The history of RFID technology. *RFID J* 2005; RFID Journal, Jan 16, 2005. Available at: http://www.rfidjournal.com/articles/view?1338 (accessed 7 August 2019).
14. Kurs A, Karalis A, Moffatt R, et al. Wireless power transfer via strongly coupled magnetic resonances. *Science* 2007; 317: 83–86.
15. Qi at wireless power consortium, www.wirelesspowerconsortium.com/member-list/ (accessed 4 October 2018).
16. Komerath N and Chowdhary G. Retail beamed power for a micro renewable energy architecture: survey. In: *2010 international symposium on electronic system design*, 20–22 December 2010. Bhubaneswar, India.
17. Griffin B and Detweiler C. Resonant wireless power transfer to ground sensors from a UAV. In: *2012 IEEE international conference on robotics and automation*, 14–19 May 2012. St Paul, MN, USA.
18. Pang Y, Zhangy Y, Guy Y, et al. Efficient data collection for wireless rechargeable sensor clusters in harsh terrains using UAVs. In: *Globecom 2014 – ad hoc and sensor networking symposium*, 8–12 Dec 2014. Austin, TX, USA.
19. Mittleider A, Griffin B and Detweiler C. Experimental robotics. In: *Experimental Analysis of a UAV-Based Wireless Power Transfer Localization System.Book: Experimental Robotics*. The 14th International Symposium on Experimental Robotics. Editors: M. Ani Hsieh, Oussama © Copyrights 2018 Khatib, Vijay Kumar. pp 357–371. Publisher: Springer, Cham
20. Detweiler C, Eiskamp M, Griffin B, et al. Unmanned aerial vehicle-based wireless charging of sensor networks. In: *Unmanned aerial vehicle-based wireless charging of sensor networks*. Book: Wireless Power Transfer Algorithms, Technologies and Applications in Ad Hoc Communication Networks. Publisher: Springer, Cham. pp 433–464.
21. Lin C, Sun Y, Wang K, et al. *Double warning thresholds for preemptive charging scheduling in wireless rechargeable sensor networks. Comput Netw* 2019; 148: 72–87.
22. Wu T, Yang P, Dai H, et al. Charging oriented sensor placement and flexible scheduling in rechargeable WSNs. In: *IEEE conference on computer communications (IEEE INFOCOM 2019)*, Paris, France, 29 April–2 May 2019.
23. Aslam N, Xia K and Usman Hadi M. Optimal wireless charging inclusive of intellectual routing based on SARSA learning in renewable wireless sensor networks. *IEEE Sensors J* 2019; May 2019, p. 99.
24. Lin C, Zhou Y, Ma F, et al. Minimizing charging delay for directional charging in wireless rechargeable sensor networks. In: *IEEE conference on computer communications (IEEE INFOCOM 2019),* Paris, France, 29 April–2 May 2019.
25. Biswas DK, Tasneem NT and Mahbub I. Optimization of miniaturized wireless power transfer system to maximize efficiency for implantable biomedical devices. In: *2019 IEEE Texas symposium on wireless and microwave circuits and systems (WMCS)*, Waco, TX, USA, 28–29 March 2019.
26. Eidaks J, Litvinenko A, Pikulins D, et al. The impact of PAPR on the wireless power transfer in IoT applications. In: *29th international conference Radioelektronika (RADIOELEKTRONIKA),* Pardubice, Czech Republic, 16–18 April 2019.
27. Sun T, Xie X and Wang Z. *Wireless power transfer for medical microsystems*. Berlin: Springer, 2013.
28. Franklin Hadley. MIT demos wireless power transmission. *MIT Tech Talk*, 13 June 2007, http://news.mit.edu/2007/techtalk51-30.pdf (accessed 14 October 2018).
29. Tipler PA and Mosca G. *Physics for scientists and engineers*. New York: W. H. Freeman, 2007.
30. Glisson TH. *Introduction to circuit analysis and design*. Berlin: Springer, 2001.
31. Meyer P. *Modeling of inductive contactless energy transfer systems*. PhD Thesis, STI, Lausanne, 2012.
32. Kim J, Kim H and Pedrotti KD. Power-efficient inductive link optimization for implantable systems. In: *Radio and wireless symposium (RWS)*, 16–19 January 2011. Phoenix, Arizona, USA.
33. Chen WK. *The circuits and filters handbook*. 2nd ed. Boca Raton: CRC Press, 2002.

34. Sonntag CLW. *Design of a variable-phase contactless energy transfer platform using air-cored planar inductor technology*. Thesis, Eindhoven University of Technology, 2010.
35. Wu HH, Hu AP, Si P, et al. A push-pull resonant converter with dual coils for transcutaneous energy transfer systems. In: *4th IEEE conference on industrial electronics and applications. ICIEA 2009*, 2009, 25–27 May 2009, Xian, China, pp.1051–1056.
36. Choi B, Nho J, Cha H, et al. Design and implementation of low-profile contactless battery charger using planar printed circuit board windings as energy transfer device. *IEEE Trans Ind Electron* 2004; 51: 140–147.
37. Phokhaphan N, Choeisai K, Noguchi K, et al. Wireless power transfer based on MHz inverter through PCB antenna. In: *1st international future energy electronics conference (IFEEC)*, 2013, 3–6 Nov 2013. Tainan, Taiwan, pp.126–130.
38. FreeRTOS, www.freertos.org/ (accessed 21 October 2018).
39. Bosshard R, Muhlethaler J, Kolar JW, et al. Optimized magnetic design for inductive power transfer coils. In: *Twenty-eighth annual IEEE applied power electronics conference and exposition (APEC)*, 2013, 17–21 Mar 2013. Long Beach, CA, USA, pp.1812–1819.
40. Karalis A, Joannopoulos JD and Soljačić M. Efficient wireless non-radiative mid-range energy transfer. *Ann Phys* 2008; 323: 34–48.
41. OpenCV (open source computer vision library), https://opencv.org/ (accessed 20 June 2019).